Wataru Ohnishi, Yuki Inada, Shungo Zen, Reon Sasaki, Yasuhiro Takada, Yuta Miyaoka, Kosuke Tsukamoto, Yasushi Yamano: Proof-of-Concept of a Fuse-Semiconductor Hybrid Circuit Breaker with a Fast Fuse Exchanger, IEEE Transactions on Power Delivery, 2022. https://doi.org/10.1109/TPWRD.2022.3202821

Proof-of-Concept of a Fuse-Semiconductor Hybrid Circuit Breaker with a Fast Fuse Exchanger

Wataru Ohnishi, *Member, IEEE,* Yuki Inada, *Member, IEEE,* Shungo Zen, *Member, IEEE,*
Reon Sasaki, Yasuhiro Takada, Yuta Miyaoka, Kosuke Tsukamoto, and Yasushi Yamano, *Member, IEEE*

***Abstract*—With the trend toward a decarbonized society where DC power networks play an important role, the importance of DC circuit breakers is increasing. In this paper, the concept of a fuse-semiconductor hybrid circuit breaker with a high-speed fuse exchanger using a high-acceleration linear motor has been presented. The authors demonstrated the feasibility of the presented concept by successfully achieving current limitation, current interruption, fuse exchange, and re-closing for fault currents with a magnitude of approximately 6.0 kA. The interruption was completed in 3.4 ms and re-closed the power system in 66.9 ms. The short interruption time can minimize damage to load equipment owing to overcurrent and power failure. The proposed operating principle has the potential to present new tradeoffs in interrupting ratings, cost, and size because a fuse, semiconductor, and varistor compensate for each other's shortcomings. Moreover, the single-usage disadvantage of the fuses was solved by the fast fuse exchanger. In addition, tradeoffs in design parameters, methods for selecting devices' ratings, and challenges to scale up are discussed in detail.**

***Index Terms*—Hybrid circuit breaker, current-limiting, fuse, semiconductor, high-speed current interruption, linear motor**

I. Introduction

DIRECT current circuit breaker (DCCB) is a critical device that is indispensable for the large-scale implementation of renewable energy [1], data centers [2], and DC railways [3] in an increasing trend shifting toward carbon neutrality. In particular, hybrid DC circuit breakers have attracted increasing attention owing to their low conduction loss and fast-breaking performance [1], [4]. Meyer et al. proposed a hybrid DCCB that combines a fast mechanical switch and a bidirectional integrated gate-commutated thyristor and demonstrated its operation in the range from 4 kA to 1.5kV [5]. Yasuoka et al. developed an arcless hybrid DCCB to interrupt DC currents below 700A [6]. Conversely, for high-voltage direct current (HVDC) circuit breakers, Jacobson et al. proposed a combination of semiconductor rectifier switches and semiconductor circuit breakers that can interrupt a rated current of 2 kA under a maximum voltage of 320 kV [7], [8]. A fault current limiter must be employed to safely interrupt a high current exceeding 10 kA [9]. DCCBs with a current-limiting facility can considerably reduce the risk of power system failures caused by fault currents and significantly improve the robustness and safety of power systems. In addition, the current limiter installation has other advantages, such as the ability to reduce the size and cost of power equipment.

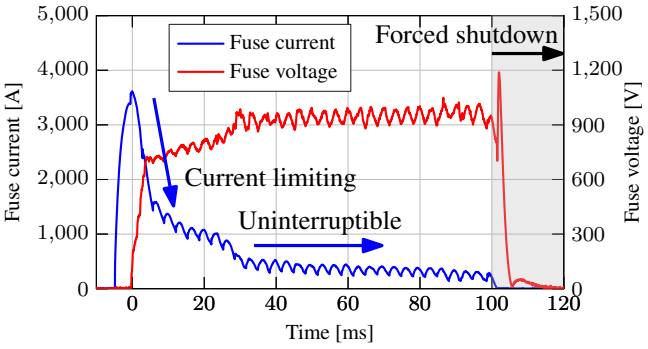

Fig. 1. Fuse only interruption test result (DC 1025V). The fuse can limit the current, but cannot be completely interrupted in this case. Finally, a backup circuit breaker was used to forcibly interrupt the circuit at 100 ms.

There are three types of current-limiting devices for fault currents: current-limiting reactors [10], [11], superconductors [12], and current-limiting fuses [13], [14]. Generally, current limiting reactors are costly and ineffective. Meanwhile, superconductors are associated with substantial operational costs to maintain cryogenic temperatures, and there is an elevated risk of burnout during current limiting. Therefore, it is advantageous to employ a current-limiting fuse as a fault current limiter.

Although the hybrid DCCBs that employ fuses as current-limiting devices have been proposed, they are combined with mechanical contacts inevitably having a jitters of 1–10 ms, making it difficult to achieve a reliable highly reproducible interrupting operation. In addition, when a fuse is solely used for interrupting operation, it is difficult to reduce the fault current to 0 A only by the current limiting action of the fuse, as shown in Fig. 1. This is especially problematic in the case of DC interruption without a current zero point. Furthermore, even if the current zero point can be temporarily achieved, conductive arcs will still exist inside the fuse, and the transient recovery voltage generated at the current zero point may cause the current to resume flowing. Thus, although fuses exhibit excellent current-limiting performance, there are issues with their own interruption performance.

W. Ohnishi, R. Sasaki, and Y. Takada are with the Department of Electrical Engineering and Information Systems, Graduate School of Engineering, The University of Tokyo, 113-8656, Japan (email: ohnishi@g.ecc.u-tokyo.ac.jp).

Y. Inada, Y. Miyaoka, K. Tsukamoto, and Y, Yamano are with the Division of Mathematics, Electronics, and Information Sciences, Saitama University, Saitama 338-8570, Japan (e-mail: inada@mail.saitama-u.ac.jp; yamano@ees.saitama-u.ac.jp).

S. Zen is with the Department of Electrical and Electronic Engineering, School of Engineering, Tokyo Institute of Technology, Tokyo 152-8552, Japan (e-mail: zen@ee.e.titech.ac.jp).

Manuscript received December 9, 2021; revised March 31, 2022, 19 June 2022, and August 20, 2022; accepted 21 August, 2022.

Therefore, our previous paper [15] has presented a fuse-semiconductor hybrid circuit breaker that has a fuse, power semiconductor switch, and varistor in parallel connection. First, fault current limiting is achieved by the fuse. When the fault current falls below a pre-set value, the power semiconductor switches (e.g., insulated gate bipolar transistors (IGBTs)) connected in parallel turn on and commute the current. Accordingly, the fuse current becomes zero, so the fuse is cooled during this time and becomes an insulator. The semiconductor then turns off, thus completing the interruption. This principle has been experimentally demonstrated at an interruption current of 1 kA and a charging voltage of 195 V. However, this configuration makes the circuit breaker "disposable" due to the single-use fuse, and hence re-closing cannot be achieved.

In this paper, we present and experimentally verify a configuration in which the old fuse is replaced by a new fuse within a short delay using a linear motor, thereby enabling quick re-closing of the circuit. The damage caused by power failures on the load can be minimized by reclosing the circuit shortly after insulation recovery. Results of experiments under two conditions of 3.6 kA and 6 kA fault currents demonstrated that the presented fuse-semiconductor hybrid circuit breaker has a high capacity for current limitation, interruption, fuse replacement, and re-closing. Under both fault current conditions, the presented hybrid circuit breaker interrupted the fault current in less than 6 ms and successfully replaced the fuse in less than 70 ms. Moreover, it was shown that the hybrid circuit breaker has high flexibility in interrupting the current by adjusting the fuse characteristics. The power supply voltages in the experiments were 300 V and 500 V. These results show the potential for low-voltage, high-current applications such as data centers, electric vehicles, and electric railways. From the above, the proof-of-concept of the fuse-semiconductor hybrid circuit breaker with the fast fuse exchanger is demonstrated.

From an engineering point of view, discussions about trade-offs in design parameters, devices' rating selection methods, and challenges for scaling up are presented. It should be emphasized that the presented circuit breaker can be applied to AC current as well as DC current. Further, while standard AC circuit breakers wait for the current zero point for interruption, the presented circuit breaker can limit and interrupt current without waiting for the current zero point.

II. Operating Principle

This section firstly introduces the configuration of the presented fuse-semiconductor hybrid circuit breaker with the fast fuse exchanger. Subsequently, the principle of interrupting rated current and fault current is introduced.

A. Overall configuration

The circuit diagram of the presented fuse-semiconductor hybrid circuit breaker is shown in Fig. 2. The total current i is measured by the control system. The fuse in Fig. 2 is mounted on a fuse exchanger shown in Fig. 3. It holds the multiple fuses and is positioned by an actuator (e.g., linear motor) driven by a servo driver.

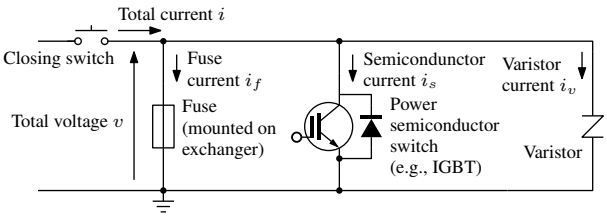

Fig. 2. Circuit diagram of the presented fuse-semiconductor hybrid circuit breaker. The operation requires the measurement of the total current i, but no other voltage or current measurements are required.

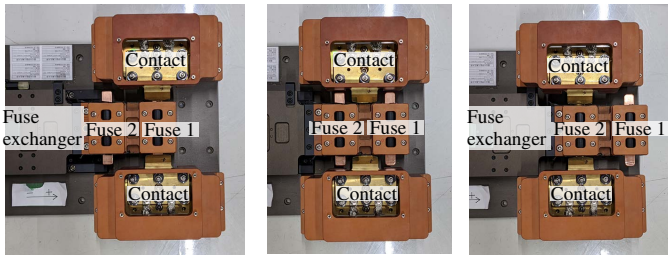

(a) Fuse 1 in use (b) Fuses disconnected (c) Fuse 2 in use

Fig. 3. Fuse exchanger with multiple fuses. Fuse positioning is accomplished by an actuator (e.g., linear motor) driven by a servo driver. This fuse exchanger not only accomplishes fuse replacement by positioning from (a) to (c) quickly, but also has a mode to temporarily disconnect the fuse in position (b) for rated current interruption, which is described in Section II-B.

Under normal conditions with the rated current flowing, the closing switch is connected, the fuse is connected, and the power semiconductor switch is off. Thus, in the presented configuration, the rated current is applied to a fuse with negligible resistance instead of a semiconductor with on-resistance. Consequently, this configuration eliminates the need for a cooling device, as is required for semiconductor circuit breakers, and thus allows for a smaller size and higher energy efficiency.

B. Rated current interruption

The presented sequence for interrupting the rated current is shown in Fig. 4. The rated current is interrupted only by the power semiconductor switch and the varistors, not by the current limiting fuse. Therefore, it is necessary to select the fuse that is not ignited at the rated current and semiconductors that are capable of interrupting the rated current.

As shown in Fig. 4(a), initially, the semiconductor switch connected in parallel to the fuse is turned off. When a command for rated current interruption is received, the power semiconductor switch first turns on as shown in Fig. 4(b). Next, the fuse is temporarily disconnect, as shown in Fig. 4(c). The presented fuse exchanger can move to a position where it is not connected to the contacts, as shown in Fig. 3(b). Then, as shown in Fig. 4(d) and (e), the rated current is interrupted by the power semiconductor switch, and the transient recovery voltage at this time is suppressed by the varistor. Finally, as shown in Fig. 4(e) and (f), the closing switch is opened after the current is completely interrupted, and then the fuse is reconnected in preparation for re-closing.

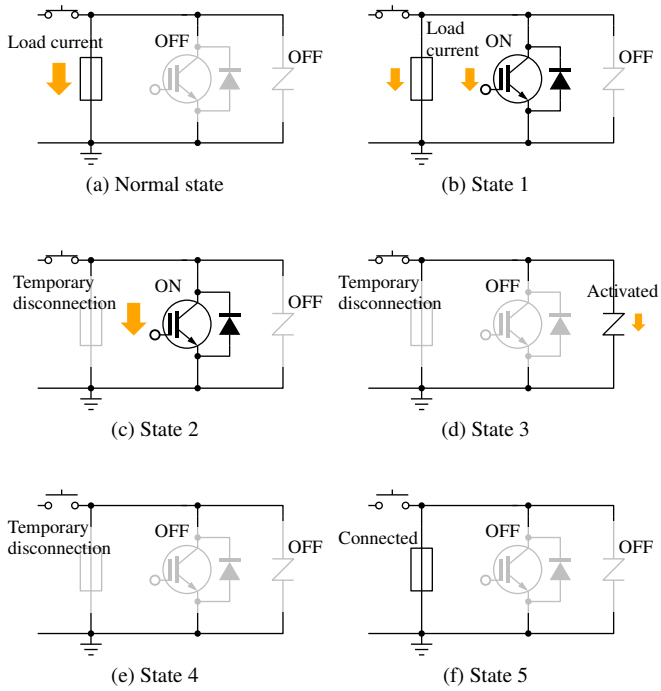

Fig. 4. Equivalent circuit diagram of the rated current interruption sequence explained in Section II-B.

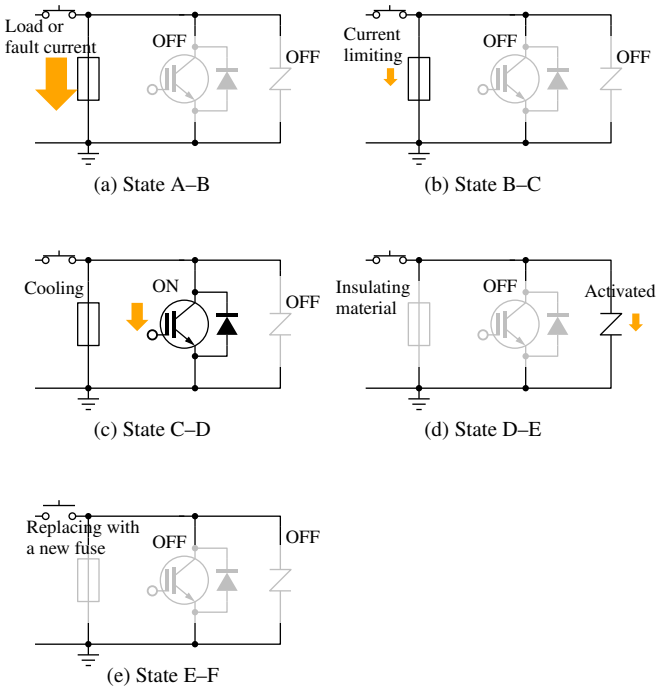

Fig. 5. Equivalent circuit diagram of the fault current interruption sequence explained in Section II-C. A description of State A–F is given in Fig. 6, which shows the the total current waveform.

C. Fault current interruption

Equivalent circuit diagram of the fault current interruption is shown in Fig. 5. A description of State A–F is given in Fig. 6, which shows the the total current waveform. The fault current limitation and interruption sequence is described in detail below.

1) Normal state before the current limiting (State A–B): Initially, the power semiconductor switch is in the off state, so the load current flows through the fuse (State A). When an accident occurs and the current rises above the designed threshold, current limiting begins (State B). This threshold is determined by the I^2t characteristic of the fuse. Note that the start of current limiting is automatic due to the self-ignition characteristics of the fuse and therefore it does not require an external signal.

2) Current limiting by fuse (State B–C): The metal element in the fuse melts due to the heat of the overcurrent, and current limiting begins. The energy of the arc discharge inside the fuse is consumed to evaporate the surrounding SiO_2 arc-extinguishing sand; thus, the arc is cooled. At this stage, the resistance of the fuse rises rapidly, causing current limiting (State B–C).

3) Current commutation by the power semiconductor switch and fuse cooling (State C–D): When the fuse current falls below a designed commutation threshold (State C), a trigger signal is sent to the pulse generator. The threshold is designed according to the current limiting performance of the fuse. A discussion on the commutation parameter design is presented in Section V-A. Consequently, the pulse generator immediately sends a turn-on signal to the power semiconductor switch and a drive flag to the servo driver. Compared to the power semiconductor switch, which is driven by an electrical time

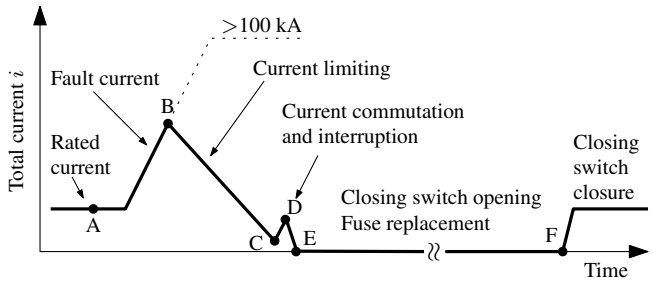

Fig. 6. Total current waveform of the fault current interruption.

constant, the servo driver is driven by a mechanical time constant; thus, it is slower, so it is possible to send the signals simultaneously. During the State C–D, there is no current flowing through the fuse because the on-resistance of the power semiconductor switch is substantially smaller than the arc resistance of the fuse. Therefore, during the State C–D, the plasma in the fuse is cooled and the fuse becomes an insulating material.

4) Power semiconductor switch turning off and energy absorption by the varistor (State D–E): At the State D, the power semiconductor switch is turned off, and the varistor connected in parallel protects the circuit during the State D–E transition such that the transient recovery voltage generated from the circuit inductance does not exceed the withstand voltage of the power semiconductor switch. The current interruption is completed at the State E.

5) Open operation of the closing switch and fuse replacement (State E–F): First, the closing switch is opened. Note that no current is flowing at this time. Next, the used fuse is replaced by the new fuse by the fuse exchanger driven by the

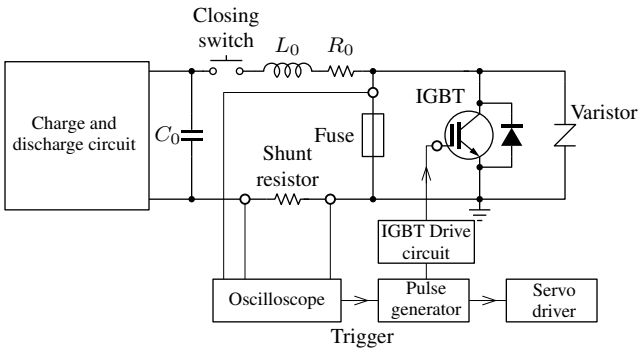

Fig. 7. Circuit diagram of the experimental setup described in Section III.

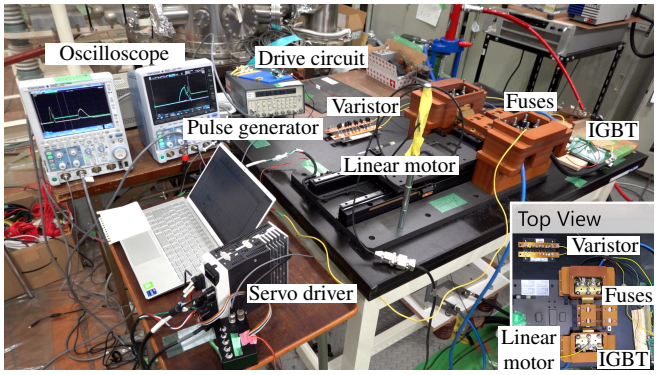

Fig. 8. Overview of the experimental setup of the fuse-semiconductor hybrid circuit breaker with fuse exchanger. A enlarged view of the fuse exchanger is shown in Fig. 9.

servo driver. By performing the fuse replacement rapidly, the system can re-close shortly after fault and reduces the damage on the load caused by power failures.

6) Re-closing (State F–): By closing the closing switch, the power grid is re-fed.

D. Type of operation and the number of fuses in the fuse exchanger

This circuit breaker is capable of Open-Close-Open (OCO) operation when equipped with two fuses. Thus, if the circuit is reclosed when the fault has not been removed, the OCO operation will be properly accomplished. In addition, when the circuit breaker has three fuses, OCO and then Close-Open operation is possible without manual fuse replacement.

III. Experimental Setup

Experimental setup is prepared for the demonstration of the presented concept. The circuit diagram and photograph of the experimental setup are shown in Figs. 7, 8 and 9. Using the experimental setup described below, a fault current interruption experiments were conducted.

A. Voltage/Current source for the fault current

The fault current was simulated by an LC circuit as shown in Fig. 7. The waveform of the short-circuit current is shown in Fig. 10, and the identified circuit parameters are $C_0 = 0.0782$ [F], $L_0 = 0.1508$ [mH], and $R_0 = 49$ [mΩ]. At a charging voltage of 500 V, the rise rate of the current was 2.6×10^6 A/s, with a peak value of 6.0 kA. At a charging voltage of 300 V, the rise rate of the current was 1.3×10^6 A/s, with a peak value of 3.6 kA.

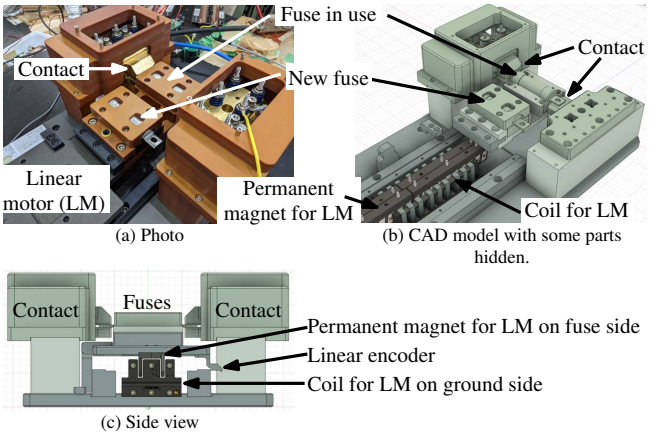

Fig. 9. Enlarged view of the fuse exchanging part. A linear motor (LM) is used in a moving magnet configuration, and the distance between the two fuses is 100 mm. A linear encoder with a resolution of 1 μm measures the position of the fuse, which is driven by the feedback control of the servo driver.

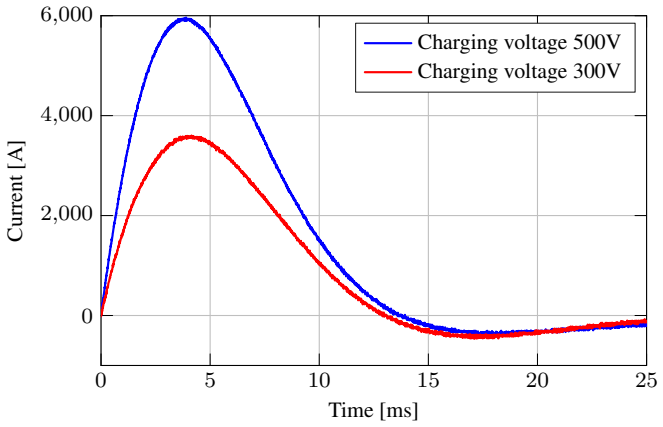

Fig. 10. Current waveform in the short-circuit test.

B. Measurement system

Total current i in Fig. 2 is need to be measured for the trigger generation for the power semiconductor switch and the servo driver. In addition, for positioning control of the fuse exchanger, it is necessary to measure the position of the fuse exchanger (e.g., by a linear encoder) and the current applied to the actuator (e.g., by a current sensor implemented in servo drivers).

The total voltage in Fig. 2 was also measured to analyze the experimental results in Section IV.

C. Fuse

In the experiments, either Fuse A (FCK2-75 from Fuji Electric FA Components & Systems Co., Ltd.) or Fuse B (PB3 from UTSUNOMIYA ELECTRIC MFG. CO., LTD.) was

TABLE I
SPECIFICATION OF THE FUSES USED IN EXPERIMENTS.

Name in paper	Product name	Manufacturer	Rated current	Rated voltage	*Total clearing I^2t
Fuse A	FCK2-75	Fuji Electric FA Components & Systems Co., Ltd.	75 A	AC500 V	113×10^3 A^2s
Fuse B	PB3	UTSUNOMIYA ELECTRIC MFG. CO., LTD.	100 A	AC500 V, DC200 V	**320×10^3 A^2s

*(Total clearing I^2t) = (Melting I^2t) + (Arcing I^2t) [16]
**from JISC8352:2015

TABLE II
SUMMARY OF THE EXPERIMENTAL RESULTS.

Fuse	Charged voltage	Fault current	Fuse arcing current	*Interruption time	*Fuse replacement time	Waveform
Fuse A	300 V	3.6 kA	3.5 kA	4.64 ms	68.2 ms	Figs. 13 and 14
Fuse A	500 V	6.0 kA	4.5 kA	5.93 ms	69.2 ms	Fig. 15
Fuse B	500 V	6.0 kA	5.7 kA	3.40 ms	66.9 ms	Fig. 16

*Interruption time and fuse replacement time are measured from the time of fuse arcing.

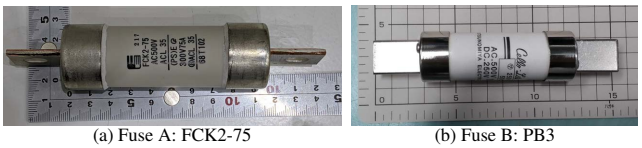

(a) Fuse A: FCK2-75 from FujiElectric FA Components & Systems Co., Ltd.

(b) Fuse B: PB3 from UTSUNOMIYA ELECTRIC MFG. CO., LTD.

Fig. 11. Fuses tested in this paper. The dimensions were based on JIS C 8314. The specifications are listed in Tab. I.

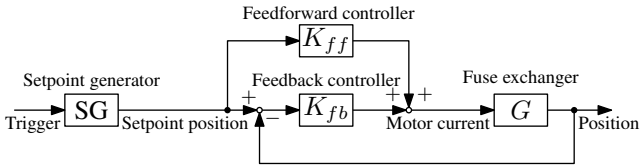

Fig. 12. Simplified block diagram of the position control system of the fuse exchanger.

used, which is shown in Fig. 11. A detailed fuse specification is listed in Tab. I.

Note that Fuse A is an AC fuse, although non-AC current shown in Fig. 10 was applied in the experiment. Fuse B is rated at DC 200 V, but 500 V was applied in the experiment. As described above, experiments were conducted under conditions that exceeded the ratings of the fuses alone.

D. Power semiconductor switch

IGBTs were selected as the power semiconductor switch. Two N-channel IGBT modules (Semikron's SEMiX603GB12E4p) with a withstand voltage of 1200 V and a maximum current capacity of 1.1 kA were connected in series. Note that 3.6 kA or 6 kA was applied in the experiments as shown in Fig. 10, which exceeds the rated current of the IGBTs alone.

E. Varistors

Varistors with the varistor voltage of 430 V and the clamping voltage of 710 V (Panasonic ERZE14A431) were used in two series and 10 parallel configurations. The clamping voltage was set below the withstand voltage of the IGBTs to protect IGBTs from overvoltage.

F. Fuse exchanger

To enable OCO operation, the fuse exchanger has two fuses, as shown in Fig. 9. Fig. 9(a) shows how the brass contacts sandwich the terminals of the fuse. A partially transparent view of the 3D CAD model is presented in Figs. 9(b) and (c).

The prepared setup was driven by a transverse magnetic flux linear motor (2L-PP09 manufactured by KOVERY CO., LTD.) with 180 N rated thrust and two rows of permanent magnets. As the linear motor is operated as a moving magnet type, the armature that requires a power cable to drive the linear motor is located on the ground side, and the moving part does not have a power cable. In addition, because of the characteristics of the transverse magnetic flux type, the mover with permanent magnets does not need to employ a back yoke made of heavy ferromagnetic materials. This contributes to reducing the weight of the mover and results in high-acceleration motion. Moreover, the transverse magnetic flux type configuration has the advantage of less magnetic attractive force and less burden on the linear guide.

The linear motor was driven by a servo driver (MCDLT35SM manufactured by Panasonic Corporation). As shown in the simplified block diagram in Fig. 12, the position control of the fuse exchanger consists of a feedforward controller for improvement of setpoint tracking and a feedback controller for disturbance suppression. The value of the nominal inertia required for the feedforward controller is obtained from modeling by measured the frequency response data. The feedback controller is a Proportional-Integral-Derivative (PID) type, and the gain is designed from the measured frequency response, taking into account the stability margin. The setpoint generator (SG in Fig. 12) implemented in the servo driver generates the setpoint position for the fuse exchanger when the servo driver receives the trigger signal from the pulse generator illustrated in Fig. 7.

IV. EXPERIMENTAL RESULTS OF THE FAULT CURRENT INTERRUPTION

Fault current interruption experiments were conducted using the experimental setup introduced in Section III. As summarized in Tab. II, two types of fuses shown in Fig. 11 were tested under the two fault current conditions of 3.6 kA and

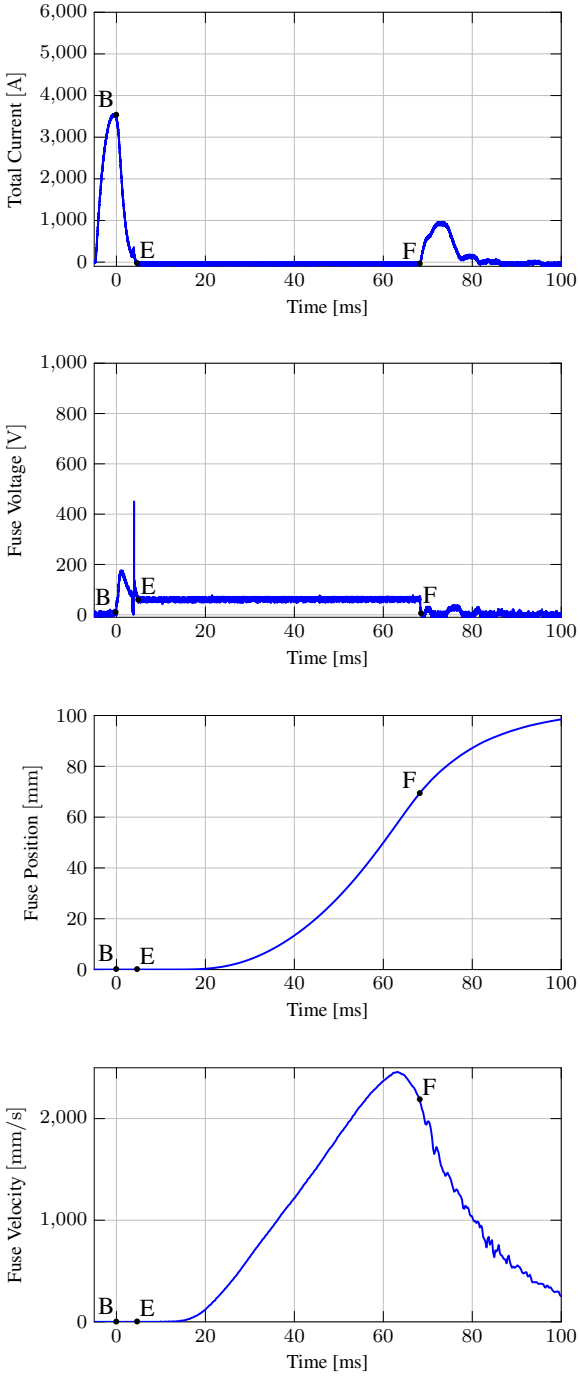

Fig. 13. Current interruption waveform of the presented fuse-semiconductor hybrid circuit breaker with the fast fuse exchanger. The fault current is set to 3.6 kA, and Fuse A is used. B–F refers to the operating principle introduced in Figs. 5, 6 and Section II. The current interruption is completed at $t = 4.64$ ms, and re-closing is completed at $t = 68.2$ [ms].

6.0 kA shown in Fig. 10. The origin of the time axis of each graph shown in Figs. 13–16 is defined as the time of arcing. As shown in Figs. 13–16, current limitation, interruption, and fuse replacement, and re-closing were successfully achieved under both fault conditions. Under all experimental conditions, the fuse elements melted. This demonstrates the efficacy and feasibility of the presented fuse-semiconductor hybrid circuit breaker with a fast fuse exchanger.

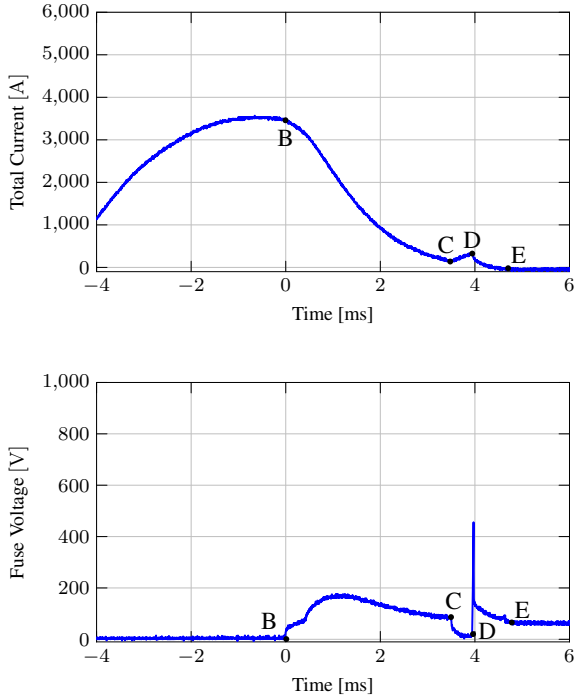

Fig. 14. Enlarged figure of Fig. 13. B–E refers to the operating principle introduced in Figs. 5, 6 and Section II. The fuse, IGBTs, and varistors operate collectively to interrupt the fault current at $t = 4.64$ [ms].

Furthermore, Figs. 15 and 16 demonstrate that the presented hybrid circuit breaker can interrupt various fault currents by selecting appropriate fuses. Fig. 15 also shows that, by integrating the IGBT, the presented hybrid circuit breaker can completely interrupt the current that cannot be interrupted solely by the fuse.

In the following experiments, under the assumption that the load insulation was quickly recovered, the closing switch is set to remain closed after the first closure, and the current flows as soon as the fuse is replaced. Note that the voltage at reclosing was lower than the initial voltage because a pre-charged LC circuit was used as the power supply device instead of a constant voltage source.

Each experimental condition is described in detail below.

A. *Fuse A with fault current 3.6 kA*

The experimental results with a charging voltage of 300 V and a fault current of 3.6 kA are shown in Figs. 13 and 14.

At $t = -4.63$ [ms], the closing switch in Fig. 2 was turned on, and the current flowing through the fuse started to increase. When the current value reached approximately 3.5 kA at the State B, the metal inside the fuse arced. As the resistance of the fuse rises rapidly after the State B, current limiting begins. Next, at the State C in Fig. 14, a trigger signal was generated by the oscilloscope shown in Fig. 2 when the fault current fell below 200 A. As a result, the IGBTs turned on, and the current was commuted through the IGBT. In this experiment, a current commutation time of 0.45 ms was set as a sufficient time to cool the fuse without exceeding the maximum current capacity of the IGBT during the State C–D. After the commutation period was completed, the IGBT

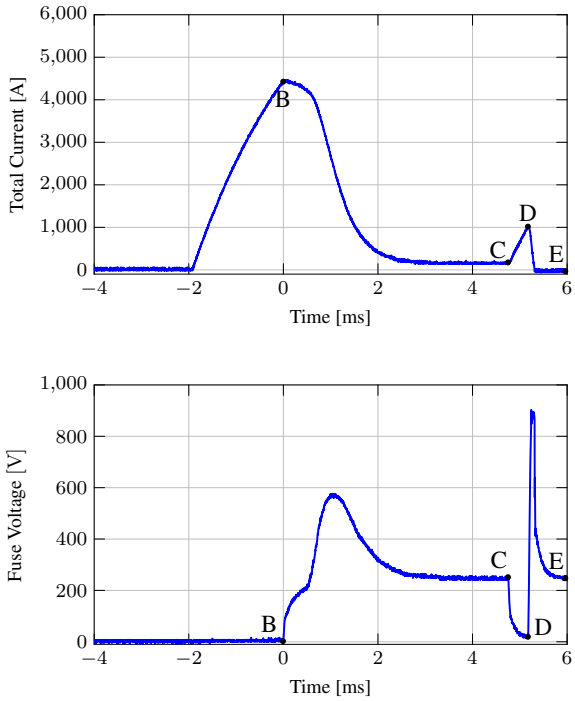

Fig. 15. Current interruption waveform. The fault current was set to 6.0 kA, and Fuse A was used. As the current continued to flow at t =2.8–4.75 [ms], it is evident that Fuse A alone cannot interrupt this fault current. However, after the State C, the fault current was completely interrupted with the aid of IGBTs. If the IGBT was not integrated, Fuse A would most likely have exploded due to thermal overload.

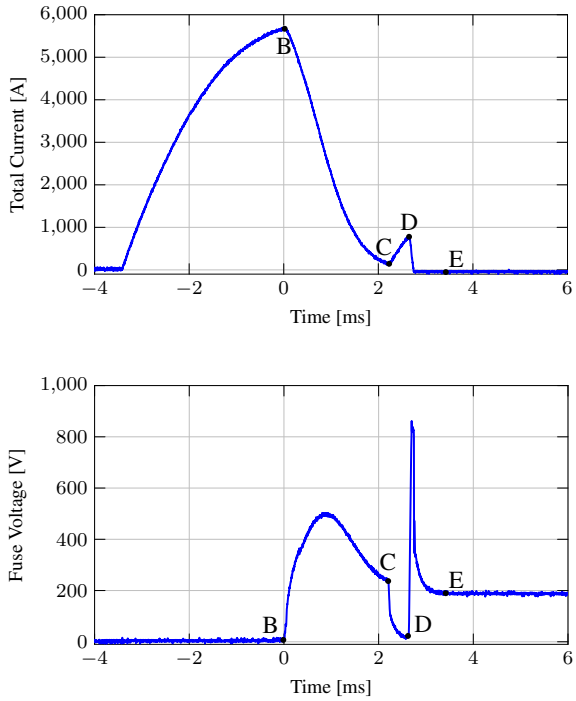

Fig. 16. Current interruption waveform. The fault current was set to 6.0 kA, and Fuse B was used. The phase from B–E corresponds to the operating principles introduced in Figs. 5, 6 and Section II.

was switched off at the State D. The varistor was activated to protect the IGBT and completely interrupt the fault current at the State E, $t = 4.64$ [ms].

In the phase between the State E and the State F, the linear motor began to move, and the fuse was accelerated at 60 $\mathrm{m/s^2}$, reaching a maximum speed of 2460 mm/s. The old fuse was then decelerated and replaced with a new fuse. While the distance between the centers of the old and new fuses was 100 mm, because of the size of the brass contacts, the new fuse moved by approximately 70 mm and then re-closed at $t = 68.2$ [ms]. Owing to the vibration of the brass contacts, a contact resistance was generated around $t = 75$ [ms]. As the power supply was a capacitor, after $t = 86.6$ [ms], all the charge had been discharged, and both the voltage and current reached zero.

B. Fuse A with fault current 6.0 kA

The experimental results for Fuse A with a charging voltage of 500 V and fault current of 6.0 kA are shown in Fig. 15. The waveforms of the linear motor motion and re-closing were similar to those in Fig. 13 and were therefore omitted.

Notably, the current value through the fuse was almost constant between $t = 2.8$–4.75 [ms]. It indicates that the arc voltage generated by of Fuse A is insufficient to exceed the power supply voltage; therefore, Fuse A cannot solely interrupted the fault current. This is because, as shown in Tab. I, Fuse A was tested under DC fault current even though it is designed for AC fault current. Therefore, this is natural since this is an out-of-specification operation. However, after the State C, it is clear that the interruption is successfully achieved with the aid of current commutation to the IGBT. If the IGBT was not integrated into the process, Fuse A would have exploded due to thermal overload.

The interruption was completed at $t = 5.93$ [ms] in the State E. The interruption time can be further shortened by setting a earlier commutation timing to the IGBT.

C. Fuse B with fault current 6.0 kA

The experimental results for Fuse B with an initial voltage of 500 V and fault current of 6.0 kA are shown in Fig. 16. The waveforms of the linear motor motion and re-closing were similar to those in Fig. 13 and were therefore omitted.

Interruption was completed at $t = 3.40$ ms at the State E. When comparing Figs. 15 and 16, Fuse B has a faster rise in arc resistance; therefore, Fuse B can limit the fault current faster.

V. Discussion

In order to make the presented circuit breaker operate according to the principle introduced in Section II, it is necessary to determine various design parameters that are trade-off relationships. The discussion in this section will summarize the trade-off and present the challenges of scaling up.

A. Commutation parameter design and its tradeoff

To interrupt the fault current under the given rising speed of the fault current, fuses and semiconductors, it is necessary to

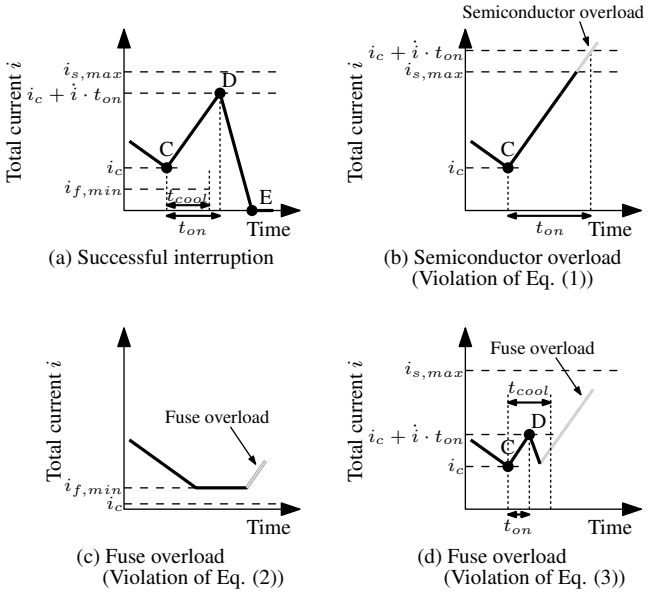

Fig. 17. Enlarged figure of Fig. 6 and the parameter constraints for interruption discussed in Section V-A. The current waveform is a simplified waveform based on a first-order approximation.

determine the starting current value of the commutation i_c, and the on-time t_{on} of the power semiconductors. Fig. 17(a) shows an enlarged waveform around the States C–E in Fig. 6. The following three inequalities must be satisfied for a successful interruption, otherwise the fuse or power semiconductor switch may explode or break.

$$i_c + \dot{i} \cdot t_{on} < i_{s,max} \tag{1}$$

$$i_{f,min} < i_c \tag{2}$$

$$t_{cool} < t_{on}, \tag{3}$$

where $\dot{i}$ denotes the di/dt factor of the fault current, $i_{s,max}$ denotes the maximum interruption current in the power semiconductor switch, $i_{f,min}$ denotes the minimum current value of the fuse after the current limiting, and t_{cool} denotes the minimum cooling time for the fuse to return to the insulator after current commutation.

Equation (1) is the constraint that the current does not exceed $i_{s,max}$ under the first-order approximation when the power semiconductor switch is in the on state. If this is not satisfied, as shown in Fig. 17(b), an overcurrent flows through the semiconductor, leading to thermal overload of the semiconductor.

Equation (2) is the constraint for the triggering of the current commutation to the semiconductor. If this is not satisfied, as shown in Fig. 17(c), the current commutation cannot be executed, leading to thermal overload of the fuse.

Equation (3) is the constraint for the minimum cooling time of the fuse to become an insulator. If this is not satisfied, as shown in Fig. 17(d), the fuse results in re-arcing, leading to thermal overload of the fuse.

These three equations represent a tradeoff between fuse and semiconductor performance. If a fuse with poor current-limiting performance, i.e., a large $i_{f,min}$, is used, $i_{s,max}$ must be increased from equations (1) and (2), leading to increased cost. In addition, if the cooling performance of the fuse is poor, i.e., a long t_{cool}, then $i_{s,max}$ must be increased as well from equations (1) and (3), which also leads to increased cost. Thus, the use of fuses with high current limiting and cooling performance can reduce the burden on semiconductors. Conversely, if a semiconductor with a large breaking current, i.e., a large $i_{s,max}$, can be developed at a low cost, the required specifications for fuse performance can be relaxed.

Furthermore, equation (1) suggests that circuit conditions with a large di/dt factor, i.e., a large $\dot{i}$, will place tighter requirements on both fuses and power semiconductor switches.

B. Selection of ratings and parameters for the system

In designing the presented hybrid circuit breaker, it is important to set the ratings of each of the fuse, semiconductor, and varistor, since each operates to cover the disadvantage of the other. The rating selection method used in this paper is summarized below.

1) Determination of the requirements as a circuit breaker: Rated current, rated voltage, di/dt rising speed of the fault current, interruption current, and the current limiting threshold (Total clearing I^2t) are evaluated for the electric power system, which the circuit breaker is installed into.

2) Selection of fuses: Fuses are selected based on the rated current, rated voltage, interruption current, Total clearing I^2t. As described in Section V-A, fuses with low current after the current limiting and a short cooling time until they become insulators can relax the requirements for the power semiconductor switch.

3) Selection of semiconductors and gate turn on time: On-time t_{on} is determined according to equation (3). Since the semiconductor must interrupt the rated current by itself, $i_{s,max}$ must be greater than the rated current, as described in Section II-B. In addition to this, select a power semiconductor switch whose value of $i_{s,max}$ satisfies equation (1).

4) Selection of gate turn off speed and varistor voltage: Fast gate turn-off generates large transient recovery voltages due to the inductance component of the system, i.e., $L_0 di/dt$. Varistors are connected in parallel to the semiconductors to protect the semiconductors and equipment from this transient recovery voltage. Therefore, the clamp voltage of the varistor must be set lower than the withstand voltage of the semiconductor devices, while the varistor voltage should be higher than the rated voltage. The gate turn-off speed must be fast enough to allow the varistor to operate in time.

5) Design of the fuse exchanger and positioning control: Increasing the number of fuses installed will reduce the labor required for manual fuse replacement. However, since the mass of the moving parts increases, the acceleration decreases from Newton's equation of motion, and the fuse replacement time increases.

In this paper, the positioning control system uses functions built into the servo driver, which simplifies the configuration and reduce the system cost. On the other hand, if the servo driver only performs current control of the motor and the current command value is generated from a separately prepared motion controller, a more dedicated control algorithm can

be applied. For example, advanced feedforward control and learning control for improved trajectory tracking performance [17], [18], [19], and feedback controller gain optimization using frequency response data for disturbance suppression [20], will enable faster fuse replacement for the same size and mass. In addition, since the fuse exchanger is a servo system with moving parts, real-time fault diagnosis and predictive maintenance are effective to ensure its reliability [24].

C. Scaling-up for interrupting current and voltage

This section summarizes the challenges to scale-up of the presented circuit breaker.

1) Higher current ratings: As described in Section V-A, it is important to use a fuse with high current limiting and cooling performance against overcurrents while it has a high current rating. If the current limiting performance of the fuse is low, the burden on the power semiconductor switch will increase, which will lead to higher costs.

Therefore, it is important to optimize the shape of fuse elements [21] and the material properties of arc-extinguishing sand [22], [23].

2) Higher voltage ratings: Voltage rating of the present setup is determined by the voltage at the State D and it was about 900 V. To increase the withstand voltage of the fuse, it is effective to lengthen the fuse or install a mechanical disconnector in series with the fuse [25]. The withstand voltage can be increased by opening the disconnector during the current limiting. To increase the withstand voltage of the power semiconductor swithes, it is effective to use the semiconductors in multiple series. Multiseries operation is easier than multiparallel operation for higher $i_{s,max}$. Furthermore, the development of new semiconductor devices, such as SiC, has resulted in improved withstand voltages.

VI. Conclusion

In this study, the proof-of-concept of a fuse-semiconductor hybrid circuit breaker with a fast fuse exchanger is demonstrated. This principle of operation has the potential to present new tradeoffs in interrupting ratings, cost, and size, because a fuse, semiconductor, varistor, and fuse exchanger compensate for each other's shortcomings. Namely, the current-limiting characteristic of the fuse helps to lower the rating of the power semiconductor switch, which has challenges in increasing the interruption current. In addition, power semiconductor switches, with their strength in interrupting, help fuses, which have a challenge in completely interrupting DC current. The presented configuration also has the advantage that a relatively small varistor is sufficient because the fuse's current-limiting effect reduces the energy of the circuit inductance. The disadvantage of the fuses being disposable is eliminated by the fast fuse exchanger. To quantitatively verify the trade-off between interruption rating, cost, and size, it is necessary to conduct further research and development to move from the current proof-of-principle stage to the industrialization stage.

One of the key factors is the performance of the fuse, so we will optimize the fuse element shapes and the material properties of the arc-extinguishing sand. In addition, a disconnector will be incorporated in series to the fuse to improve the withstand voltage.

Acknowledgment

This study was partially supported by the New Energy and Industrial Technology Development Organization (NEDO) 21501372-0, JSPS KAKENHI 21K14179, Nagamori Foundation, Research Foundation for the Electrotechnology of Chubu, and Power Academy. The author also acknowledges the technical assistance from Dr. Houng-Joong Kim from KOVERY CO., LTD.

References

[1] F. Mohammadi, K. Rouzbehi, M. Hajian, K. Niayesh, G. B. Gharehpetian, H. Saad, M. Hasan Ali, and V. K. Sood, "HVDC Circuit Breakers: A Comprehensive Review," *IEEE Transactions on Power Electronics*, vol. 36, no. 12, pp. 13 726–13 739, 2021.

[2] S. Hay, C. Cleary, G. Mcfadzean, J. Mcgray, and N. Kelly, "MVDC technology study - market opportunities and economic impact," no. February, pp. 1–126, 2015.

[3] A. Verdicchio, P. Ladoux, H. Caron, and C. Courtois, "New Medium-Voltage DC Railway Electrification System," *IEEE Transactions on Transportation Electrification*, vol. 4, no. 2, pp. 591–604, 2018.

[4] X. Pei, O. Cwikowski, D. S. Vilchis-Rodriguez, M. Barnes, A. C. Smith, and R. Shuttleworth, "A review of technologies for MVDC circuit breakers," in *42nd Annual Conference of the IEEE Industrial Electronics Society*, 2016, pp. 3799–3805.

[5] J. M. Meyer and A. Rufer, "A DC hybrid circuit breaker with ultra-fast contact opening and integrated gate-commutated thyristors (IGCTs)," *IEEE Transactions on Power Delivery*, vol. 21, no. 2, pp. 646–651, 2006.

[6] C. Ou, H. Yinming, and K. Yasuoka, "New Configuration of Contacts for Increasing the Threshold Current of Arc-Free Commutation in a DC Hybrid Switch," *IEEE Transactions on Components, Packaging and Manufacturing Technology*, vol. 10, no. 8, pp. 1320–1327, 2020.

[7] M.Callavik, A.Blomberg, J.Hafner, and B.Jacobson, "Hybrid DC Breaker—An innovation breakthrough enabling reliable HVDC grids," *ABB Grid Systems*, 2012.

[8] A. Hassanpoor, J. Häfner, and B. Jacobson, "Technical Assessment of Load Commutation Switch in Hybrid HVDC Breaker," *IEEE Transactions on Power Electronics*, vol. 30, no. 10, pp. 5393–5400, 2015.

[9] U. Amir Khan, J. G. Lee, F. Amir, and B. W. Lee, "A Novel Model of HVDC Hybrid-Type Superconducting Circuit Breaker and Its Performance Analysis for Limiting and Breaking DC Fault Currents," *IEEE Transactions on Applied Superconductivity*, vol. 25, no. 6, pp. 1–9, 2015.

[10] H. Radmanesh, S. H. Fathi, and G. B. Gharehpetian, "Novel high performance DC reactor type fault current limiter," *Electric Power Systems Research*, vol. 122, pp. 198–207, 2015.

[11] A. Mokhberdoran, D. Van Hertem, N. Silva, H. Leite, and A. Carvalho, "Multiport Hybrid HVDC Circuit Breaker," *IEEE Transactions on Industrial Electronics*, vol. 65, no. 1, pp. 309–320, 2018.

[12] H. J. Boenig and D. A. Paice, "Fault current limiter using a superconducting coil," *IEEE Transactions on Magnetics*, vol. 19, no. 3, pp. 1051–1053, 1983.

[13] L. Kojovic and S. Hassler, "Application of current limiting fuses in distribution systems for improved power quality and protection," *IEEE Transactions on Power Delivery*, vol. 12, no. 2, pp. 791–800, 1997.

[14] L. Kojovic, S. Hassler, K. Leix, C. Williams, and E. Baker, "Comparative analysis of expulsion and current-limiting fuse operation in distribution systems for improved power quality and protection," *IEEE Transactions on Power Delivery*, vol. 13, no. 3, pp. 863–869, 1998.

[15] S. Zen, Y. Inada, W. Ohnishi, Y. Fukai, N. Takayasu, M. Maeyama, and Y. Yamano, "Prototype Current-Limiting Hybrid DC Circuit Breaker Incorporating a Fuse and a Semiconductor Device," *IEEE Transactions on Power Delivery*, vol. 36, no. 4, pp. 2231–2233, 2021.

[16] Littelfuse, *FUSEOLOGY*. https://www.littelfuse.com/~/media/automotive/catalogs/littelfuse_fuseology.pdf

[17] W. Ohnishi, T. Beauduin, and H. Fujimoto, "Preactuated Multirate Feedforward Control for Independent Stable Inversion of Unstable Intrinsic and Discretization Zeros," *IEEE/ASME Transactions on Mechatronics*, vol. 24, no. 2, pp. 863–871, 2019.

[18] L. Aarnoudse, W. Ohnishi, M. Poot, P. Tacx, N. Strijbosch, and T. Oomen, "Control-Relevant Neural Networks for Intelligent Motion Feedforward," in *IEEE International Conference on Mechatronics*, 2021.
[19] W. Ohnishi, N. Strijbosch, and T. Oomen, "Multirate State Tracking for Improving Intersample Behavior in Iterative Learning Control," in *IEEE International Conference on Mechatronics*, 2021.
[20] X. Wang, W. Ohnishi, and T. Koseki, "Frequency Response Data Based Disturbance Observer Design: With Application to a Nonminimum Phase Motion Stage," *IEEE/ASME Transactions on Mechatronics*, 2022.
[21] Y. Ishikawa, K. Hirose, M. Asayama, Y. Yamano, and S. Kobayashi, "Dependence of current interruption performance on the element patterns of etched fuses," in *8th International Conference on Electric Fuses and their Applications*, 2007, pp. 51–56.
[22] W. Bussière, "Influence of sand granulometry on electrical characteristics, temperature and electron density during high-voltage fuse arc extinction," *Journal of Physics D: Applied Physics*, vol. 34, no. 6, pp. 925–935, 2001.
[23] N. Kodama, K. Nakamura, Y. Yokomizu, A. Takahashi, and N. Yamamura, "DC Arc Resistance Rise by PMMA Cylinder Ablation with Arc Shrinking in Silica Sand Filling Space," *IEEJ Transactions on Electrical and Electronic Engineering*, vol. 16, no. 12, pp. 1679–1686, 2021.
[24] K. Classens, S. Verbeek, W. P. M. H. Heemels, and T. Oomen, "Joint Estimation of Additive and Parametric Faults : A Model-Based Fault Diagnosis Approach towards Predictive Maintenance," in *11th IFAC Symposium on Fault Detection, Supervision, and Safety of Technical Processes (SAFEPROCESS 2022)*, 2022.
[25] Y. Inada, Y. Yamano, M. Maeyama, S. Zen, and W. Ohnishi, "CURRENT INTERRUPTION DEVICE AND CURRENT INTERRUPTION METHOD," 2020/09/15. PCT/JP2020/034978. 2021/03/25. WO 2021/054338. 2021.

Wataru Ohnishi (S'13-M'18) received the B.E., M.S., and Ph.D. degrees from The University of Tokyo, Japan in 2013, 2015, and 2018, respectively. Presently, he is an assistant professor with the Department of Electrical Engineering and Information Systems, Graduate School of Engineering, The University of Tokyo. He held a visiting position at the Eindhoven University of Technology. His research interests include high-precision motion control and optimization. He is a member of IEEJ.

Yuki Inada (M'15) was born in Japan in 1985. He received the B.S. degree in electronic engineering from the Tokyo Institute of Technology, Tokyo, Japan, in 2009, and the M.S. and Dr. degrees in electrical engineering from The University of Tokyo, Tokyo, in 2011 and 2014, respectively. He was a Project Assistant Professor with The University of Tokyo in 2014. Since 2015, he has been working at Saitama University, Saitama, as an Assistant Professor. His research interests include plasma diagnostic techniques, arc interruption phenomena, and plasma application technology.

Shungo Zen (M'16) received the B.E., M.E., and Ph.D degrees from the University of Tokyo, Kashiwa, Japan, in 2007, 2011, and 2016, respectively, all in electrical engineering. He is currently an Assistant Professor with the Department of Electrical and Electronic Engineering, Tokyo Institute of Technology, Tokyo. His current research interests include dc hybrid switch technologies and atmospheric pressure plasma applications. Dr. Zen is a member of the Institute of Electrical Engineers of Japan.

Reon Sasaki received the B.E. degree in electrical engineering from The University of Tokyo, Tokyo, Japan, in 2021. His research interest includes high-precision motion control.

Yasuhiro Takada received the B.E. degree in electrical engineering from Tokyo University of Science, Tokyo, Japan, in 2007. Presently, he is a technical specialist with the Department of Electrical Engineering and Information Systems, Graduate School of Engineering, The University of Tokyo.

Yuta Miyaoka received the B.E. degree in electrical engineering from Saitama University, Saitama, Japan, in 2021.

Kosuke Tsukamoto received the B.E. degree in electrical engineering from Saitama University, Saitama, Japan, in 2021.

Yasushi Yamano (M'15) was born on June 16, 1970. He received the B.Eng. and M.Eng. degrees from the Nagoya Institute of Technology, Nagoya, Japan, in 1994 and 1996, respectively, and the Dr. Eng. degree from Nagoya University, Nagoya, in 2000. He has been a Research Associate since 2000 and an Associate Professor since 2009 with Saitama University, Saitama, Japan. His research interests include vacuum discharge and insulation technology and fuse technology.